GEOPHYSICS, VOL. 80, NO. 3 (MAY-JUNE 2015); P. D221–D235, 8 FIGS., 2 TABLES.
10.1190/GEO2014-0307.1

Downloaded 04/06/15 to 112.10.114.108. Redistribution subject to SEG license or copyright; see Terms of Use at http://library.seg.org/

Seismic reflection dispersion due to wave-induced fluid flow in heterogeneous reservoir rocks

Luanxiao Zhao[1], De-hua Han[2], Qiuliang Yao[3], Rui Zhou[2], and Fuyong Yan[2]

ABSTRACT

We have investigated the impact of wave-induced fluid flow, including Biot flow and mesoscopic flow, on the signatures of seismic reflectivity in heterogeneous reservoir rocks. We have incorporated the dynamic poroelastic responses of mesoscopic flow into the classical Biot theory. The resulting effective Biot media could capture the characteristics of velocity dispersion and wave attenuation in heterogeneous poroelastic media. On the basis of this effective Biot media, an approach was developed to compute the poroelastic reflection at arbitrary angles and frequencies from the boundary of two heterogeneous porous media. The computed poroelastic reflections not only depended on the elastic properties' contrast and incident angle, but also relied on the fluid mobility and observational frequency. For a typical sand-shale reflector, with the given rock and fluid properties, we found that the effect of mesoscopic flow causes P-wave reflection amplitude variations with the frequency being as high as 40% and a maximum phase shift as high as 16° at the seismic exploration frequency band. In addition, it was found that the amplitude variation with offset intercept and the gradient at the poroelastic interface were impacted by the mesoscopic flow and had a decreasing trend with frequency. Therefore, ignoring the impact of mesoscopic flow could possibly lead to uncertainty in seismic imaging as well as quantitative interpretation of reservoir properties. In comparison, the Biot flow-induced seismic dispersion effect, which occured at a very high-frequency range, was almost negligible.

INTRODUCTION

Seismic waves propagating in heterogeneous porous media create fluid pressure gradients and consequently induce fluid flow. During the process of fluid flow, viscous-inertial loss takes place and dissipates mechanical energy into heat, which is responsible for the intrinsic attenuation of seismic waves (Aki and Richards, 1980; Müller et al., 2010). The wave-induced fluid flow typically affects wave propagation characteristics (Biot, 1956a, 1956b, 1962; Pride and Berryman, 2003a, 2003b), and hence it affects the behavior of reflection coefficients. The most pronounced influence is that the reflection coefficients are frequency dependent, known as *reflection dispersion*. It is of considerable interest to understand the poroelastic reflection signatures, which are believed to have potential in revealing reservoir properties, such as saturation content and flow characteristics. Furthermore, an extensive investigation on the poroelastic reflection at a wide frequency range is critical to help us realize the physical discrepancy standing behind the different geophysical measurements at various scales, which typically include the surface seismic data (10^{0-2} Hz), virtual seismic profile (VSP) data (10^{2-3} Hz), sonic logs (10^{3-4} Hz), and lab measurements (10^{0-6} Hz). The present work contributes to quantifying the impact of wave-induced fluid flow on the signatures of reflection coefficients in heterogeneous reservoir rocks.

In the past decades, dissipation-related seismic attributes already have been used to interpret seismic data as hydrocarbon indicators or to map reservoir properties (e.g., Taner et al., 1979; Castagna et al., 2003; Ebrom, 2004; Hofmann, 2006; Odebeatu et al., 2006). Nevertheless, most of those applications are empirical and qualitative. Based on the analysis of the experimental and field seis-

Manuscript received by the Editor 5 July 2014; revised manuscript received 15 December 2014; published online 30 March 2015.
[1]Tongji University, State Key Laboratory of Marine Geology, Shanghai, China and University of Houston, Department of Earth and Atmospheric Sciences, Houston, Texas, USA. E-mail: zhaoluanxiao@gmail.com.
[2]University of Houston, Department of Earth and Atmospheric Sciences, Houston, Texas, USA. E-mail: dhan@uh.edu; julian_yao@hotmail.com; zhourui2058@gmail.com; yanfyon@yahoo.com.
[3]Formerly University of Houston, Department of Earth and Atmospheric Sciences, Houston, Texas, USA; presently Halliburton Consulting and Project Management, Houston, Texas, USA.
© 2015 Society of Exploration Geophysicists. All rights reserved.

Downloaded 04/06/15 to 112.10.114.108. Redistribution subject to SEG license or copyright; see Terms of Use at http://library.seg.org/

mic data, Korneev et al. (2004) and Goloshubin et al. (2001, 2006) report that the seismic reflection from a fluid-saturated layer shows a clear frequency-dependent amplitude response, and they further demonstrate that the theoretical formulation with a diffusive term gives a reasonable match with the physical modeling data. Chapman et al. (2006) systematically investigate the impacts of hydrocarbon-related dispersion and attenuation on the seismic reflections and conclude that such influences are intimately associated with the amplitude variation with offset (AVO) behavior at the interface. Generally, much of the progress related to the frequency-dependent seismic analysis has been driven by the development of spectral decomposition methods, which break down the seismic reflection signal into its component frequencies (Chakraborty and Okaya, 1995; Partyka et al., 1999; Castagna et al., 2003).

From a theoretical point of view, many authors (Geertsma and Smit, 1961; Stoll, 1977; Dutta and Odé, 1983; Bourbié et al., 1987; Gurevich and Schoenberg, 1999; Gurevich et al., 2004) study the seismic reflection coefficients at an interface between two porous homogeneous media. The slow P-wave related to the fluid pressure diffusion is generated at the interface of poroelastic contact. Based on their calculations, the inelastic energy loss for reflection amplitudes is only significant at a very high frequency. Physically, this is understandable because with typical subsurface rock and fluid properties, the relative fluid flow with respect to the solid, namely, global flow due to wavelength scale pore-pressure equilibration, becomes negligible at a low frequency. Meanwhile, the reflections at the interface between a liquid and a liquid-saturated porous solid are also investigated extensively by Deresiewicz and Rice (1960), Denneman et al. (2002), Gurevich et al. (2004), Rubino et al. (2006), and Bouzidi and Schmitt (2012). The deviation of poroelastic reflections from the elastic one can be significant at an interface between a free fluid (water) and gas-saturated porous medium because of the large contrast in the compressibility of water and gas (Denneman et al., 2002; Gurevich et al., 2004).

However, those situations are too ideal to permit the application of the theory to most subsurface sedimentary rocks, which are generally heterogeneous by their very nature. Consequently, it is essential to understand the poroelastic reflection signatures in realistic heterogeneous porous rocks, where the effect of velocity dispersion and wave attenuation becomes more prominent. As we know, in partially saturated rock or in fully saturated elastically heterogeneous rock, the viscous loss is mainly caused by an internal equilibration that takes places with fluid flowing from the more compliant high-pressure regions to the relatively stiffer low-pressure regions (Batzle et al., 2006). Based on the heterogeneities of various scale, such local flow can be categorized as *squirt flow* and *mesoscopic flow*. Squirt flow typically occurs at the microscopic pore scale (O'Connell and Budiansky, 1974; Mavko and Nur, 1975; Mavko and Jizba, 1991; Dvorkin et al., 1995; Chapman et al., 2002; Tang, 2011), whereas mesoscopic flow is created by the heterogeneities on a scale much larger than the typical pore size but smaller than the wavelength (White, 1975; Dutta and Odé, 1979a, 1979b; Gelinsky and Shapiro, 1997; Gurevich et al., 1997; Shapiro and Müller, 1999; Pride and Berryman, 2003a, 2003b; Müller and Gurevich, 2004, 2005; Carcione and Picotti, 2006; Müller et al., 2007; Carcione et al., 2013). Generally, squirt flow is usually considered to be important at ultrasonic frequencies, whereas mesoscopic flow is increasingly considered as the dominant cause of fluid-related attenuation in the seismic exploration band (Pride et al., 2004; Müller et al., 2010).

With regard to the influences of local flow on the reflection coefficients, Quintal et al. (2009) and Ren et al. (2009) combine the analytical solution of White's 1D model (White, 1975; Carcione and Picotti, 2006) and the analytical expression of reflection coefficient in viscoelastic media to analyze the reflection dispersion signatures in a thinly layered, partially saturated reservoir with a nondispersive overburden. Alternately, rather than considering the poroelastic behavior due to the complex interaction between fluid and solid, many authors report the impact of Q-contrast on the reflection amplitude and phase in viscoelastic media theoretically (White, 1965; Bourbié, 1983; Lines et al., 2008; Morozov, 2011) and experimentally (Bourbié and Nur, 1984; Lines et al., 2012).

In general, the theoretical formulation for the reflection coefficients from the boundary of heterogeneous poroelastic media as a function of material properties, incident angle, and frequency is very complicated. In this study, we seek to present an effective procedure to calculate the poroelastic reflection coefficients at arbitrary incident angles and frequencies. In addition, it is well known that the Biot flow and local flow always take place simultaneously when heterogeneities are present. However, studying the reflection dispersion signatures including the effects of Biot flow and local flow simultaneously is sparsely documented. In this paper, to preserve the theoretical generality, the computed poroelastic reflection will incorporate the effect of local flow as well as Biot flow.

To characterize the reflection dispersion signatures, the first essential question to be addressed is how to describe the heterogeneous porous media that waves propagate through. Many poroelastic models have been proposed to explain velocity dispersion and wave attenuation characteristics due to the inertial fluid effect. In this paper, emphasis will be placed on the double-porosity dual-permeability (DPDP) model developed by Berryman and Wang (1995, 2000), Pride and Berryman (2003a, 2003b), and Pride et al. (2004). There are several reasons to choose the double-porosity model. First of all, it represents a general framework to model wave propagation through heterogeneous porous structures, without placing any restriction on the mesoscopic geometry of the heterogeneity (Pride et al., 2004). Second, to highlight the effect of intrinsic loss and dispersion on reflection dispersion in the seismic frequency band, the geologic heterogeneities here will be specified as being of mesoscopic scale. Moreover, Pride et al. (2004) show that this theory can also be designed to simulate the dispersion effect associated with patchy saturation and squirt flow.

The content of this paper is structured as follows: First, we briefly review wave dispersion and attenuation characteristics using the DPDP model. Next, we present how to use an effective procedure to calculate the poroelastic reflection in heterogeneous porous media. Following this section, a typical sand-shale reflector will be presented to quantitatively analyze the seismic reflection dispersion characteristics in terms of its magnitude and phase angle. The potential implications for reservoir characterization will also be explored. Finally, we end with discussions and conclusions.

THEORY

Double-porosity dual-permeability model

The DPDP model often represents a more general framework to explain the velocity dispersion and attenuation due to mesoscopic

Downloaded 04/06/15 to 112.10.114.108. Redistribution subject to SEG license or copyright; see Terms of Use at http://library.seg.org/

fluid flow. Heterogeneous porous media is described as a composite that consists of two distinct porous phases, exhibiting contrasting hydraulic and elastic properties but saturated by a single fluid phase. One typical example to elucidate the double-porosity model is a fractured reservoir: The fracture or crack porosity normally occupies small portions of the volume, but with higher compressibility and permeability than those of the host rock.

The governing equations for DPDP in the frequency domain are given as (Pride and Berryman, 2003a, 2003b; Pride et al., 2004)

$$\nabla \times \boldsymbol{\tau}^D - \nabla P_c = -i\omega(\rho \mathbf{v} + \rho_f \mathbf{q_1} + \rho_f \mathbf{q_2}), \tag{1}$$

$$\begin{bmatrix} \mathbf{q_1} \\ \mathbf{q_2} \end{bmatrix} = -\frac{1}{\eta} \begin{bmatrix} \kappa_{11} & \kappa_{12} \\ \kappa_{12} & \kappa_{22} \end{bmatrix} \begin{bmatrix} \nabla \bar{p}_{f1} - i\omega\rho_f \boldsymbol{\nu} \\ \nabla \bar{p}_{f2} - i\omega\rho_f \boldsymbol{\nu} \end{bmatrix}, \tag{2}$$

$$\begin{bmatrix} \nabla \times \boldsymbol{\nu} \\ \nabla \times \mathbf{q_1} \\ \nabla \times \mathbf{q_2} \end{bmatrix} = i\omega \begin{bmatrix} a_{11} & a_{12} & a_{13} \\ a_{12} & a_{22} & a_{23} \\ a_{13} & a_{23} & a_{33} \end{bmatrix} \begin{bmatrix} P_c \\ \bar{p}_{f1} \\ \bar{p}_{f2} \end{bmatrix} + i\omega \begin{bmatrix} 0 \\ \zeta_{\text{int}} \\ -\zeta_{\text{int}} \end{bmatrix}, \tag{3}$$

$$-i\omega\zeta_{\text{int}} = \gamma(\omega)(\bar{p}_{f1} - \bar{p}_{f2}), \tag{4}$$

$$-i\omega\boldsymbol{\tau}^D = [G(\omega) - i\omega g(\omega)]\left[\nabla\boldsymbol{\nu} + (\nabla\boldsymbol{\nu})^T - \frac{2}{3}\nabla \times \boldsymbol{\nu}\mathbf{I}\right]. \tag{5}$$

Here, phases 1 and 2 refer to the host phase and heterogeneity phase, respectively, τ^D and P_c represent the total average deviatoric stress and total average confining pressure acting on the averaging volume of porous composite, respectively, $\boldsymbol{\nu}$ denotes the average solid-grain velocity, q_i denotes the macroscopic fluid flux across phase i, $\kappa_{ij}(i, j = 1,2)$ describes the dynamic permeability of the two phases as well as their coupling, $\bar{p}_{fi}$ indicates the average fluid pressure within phase i, ζ_{int} indicates the increment of fluid content due to internal mesoscopic flow where fluid pressure is relaxed between phases 1 and 2, and $G(\omega)$ is the Hilbert transform of $g(\omega)$ characterizing the dispersion features of shear modulus of the porous composite. The constants a_{ij} correspond to the high-frequency responses without internal fluid pressure relaxation and are expressed with the following relations (Pride et al., 2004):

$$a_{11} = 1/K_d, \quad a_{22} = \frac{v_1\alpha_1}{K_d^1}\left(\frac{1}{B_1} - \frac{\alpha_1(1-Q_1)}{1-K_d^1/K_d^2}\right),$$

$$a_{33} = \frac{v_2\alpha_2}{K_d^2}\left(\frac{1}{B_2} - \frac{\alpha_2(1-Q_2)}{1-K_d^2/K_d^1}\right), \quad a_{12} = v_1 Q_1 \alpha_1 / K_d^1,$$

$$a_{13} = v_2 Q_2 \alpha_2 / K_d^2,$$

$$a_{23} = -\frac{\alpha_1\alpha_2 K_d^1/K_d^2}{(1-K_d^1/K_d^2)^2}\left(\frac{1}{K} - \frac{v_1}{K_d^1} - \frac{v_2}{K_d^2}\right),$$

where the Q_i are given by

$$Q_1 = \frac{1}{v_1}\frac{1-K_d^2/K_d}{1-K_d^2/K_d^1} \text{ and } Q_2 = \frac{1}{v_2}\frac{1-K_d^1/K_d}{1-K_d^1/K_d^2}. \tag{6}$$

Here, v_1 and v_2 are the volume fractions of phases 1 and 2 within an averaging volume of the composite, K_d^1 and K_d^2 are the bulk moduli of the drained rock frames of phases 1 and 2, respectively, K_d is the drained bulk modulus of the double-porosity composite, α_1 and α_2 are the Biot's constants of phases 1 and 2, respectively, and B_1 and B_2 are the Skempton's coefficient of phases 1 and 2, respectively.

Each set of the governing equation has explicit physical significance. Note that the above equations characterize the signatures of three types of fluid flow: two types of external fluid flow and one type of internal fluid flow. Equation 2 represents the generalized Darcy's law corresponding to the external fluid flow at the macroscopic scale. Equation 4 gives the transport law to characterize the internal mesoscopic flow, which results in the main viscous loss for the heterogeneous poroelastic system. In addition, equation 1 represents the conservation of the momentum, and equations 3 and 5 are the generalized compressibility law. Further analysis of these equations suggests that there exist three P-waves and a single S-wave (Berryman and Wang, 2000; Pride et al., 2004). The first type of P-wave represents the conventional fast P-wave, and the other two slow P-wave modes correspond to fluid pressure diffusion due to the external fluid flow.

The frequency-dependent relaxation coefficient $\gamma(\omega)$ in equation 4, which essentially controls the mesoscopic flow characteristic, is defined as (Pride et al., 2004)

$$\gamma(\omega) = \gamma_m\sqrt{1 - i\frac{\omega}{\omega_m}}, \tag{7}$$

where

$$\gamma_m = -\frac{\kappa_1 K_1^d}{\eta L_1^2}\left(\frac{a_{12} + B_0(a_{22} + a_{33})}{R_1 - B_0/B_1}\right)[1 + O(\kappa_1/\kappa_2)], \tag{8}$$

$$\omega_m = \frac{\eta B_1 K_1^d}{\kappa_1\alpha_1}\left(\gamma_m\frac{V}{S}\right)^2\left[1 + \sqrt{\frac{\kappa_1 B_2 K_2^d \alpha_1}{\kappa_2 B_1 K_1^d \alpha_2}}\right]. \tag{9}$$

Here, κ_1 and κ_2 are the permeability of phases 1 and 2, respectively, η is the fluid viscosity, B_0 is the Skempton's coefficient of the double-porosity composite, and R_1 indicates the ratio of the average confining pressure in phase 1 to the external pressure applied to the double-porosity composite. Two geometric parameters L_1 and V/S describe the shape and size of the heterogeneity: S is the surface area of the interface between the two phases in each volume V of composite, and L_1 describes the phase 1 length with pore fluid pressure gradient that relaxes in the final approach to fluid pressure equilibrium (Pride et al., 2004). Note that the parameters controlling the characteristic frequency are mainly dependent on the properties of host phase 1, and hence host phase 1 actually determines the timing of the fluid pressure diffusion.

Effective Biot media

To illustrate the effects of the wave-induced flow on the reflection of seismic waves, we treat the simplified problem of reflection and transmission of a plane compressional seismic wave incident with an oblique angle at a plane interface between two heterogeneous porous media in the upper and lower half-space. If the DPDP model is used to describe the wave characteristics in heterogeneous porous materials, the incident plane P-wave will generate four reflected wave modes and four transmitted wave modes: fast P-wave,

Downloaded 04/06/15 to 112.10.114.108. Redistribution subject to SEG license or copyright; see Terms of Use at http://library.seg.org/

converted S-wave, first-kind slow P-wave, and second-kind slow P-wave (Berryman and Wang, 1995, 2000; Pride et al., 2004; Dai and Kuang, 2006). Mathematically, solving such a problem of plane-wave reflection and transmission in double-porosity media becomes extremely tedious because there is a requirement of eight boundary conditions to constrain the solutions of the reflection and transmission coefficients. Consequently, it was deemed necessary to describe the heterogeneous porous media in a simplified way.

Here, we reduce the double-porosity theory to the effective single-porosity Biot theory suggested by Pride et al. (2004). With the assumption that the heterogeneity phase is totally embedded in the host phase, the fluid motion relative to the solid skeleton of the heterogeneity phase vanishes. The effect of internal flow is included in the effective drained bulk modulus, which can be derived from the original parameters of the double-porosity model. The frequency-dependent poroelastic moduli in effective Biot media are given as

$$\frac{1}{K_d^*} = a_{11} - \frac{a_{13}^2}{a_{33} - \gamma/i\omega}, \tag{10}$$

$$B = \frac{-a_{12}(a_{33} - \gamma/i\omega) + a_{13}(a_{23} + \gamma/i\omega)}{(a_{22} - \gamma/i\omega)(a_{33} - \gamma/i\omega) - (a_{23} + \gamma/i\omega)^2}, \tag{11}$$

$$\frac{1}{K_u^*} = \frac{1}{K_d^*} + B\left(a_{12} - \frac{a_{13}(a_{23} + \gamma/i\omega)}{a_{33} - \gamma/i\omega}\right). \tag{12}$$

Here, K_d^* is the effective drained bulk modulus, B is the effective Skempton's coefficient, and K_u^* is the effective undrained bulk modulus. For a better understanding, assuming that if the average fluid pressure across the double-porosity composite under the drained condition is not changed, but in order for the internal pore pressure to be equilibrated, the total volumetric response should be redefined as inelastic or frequency dependent. In fact, K_d^* represents the effective elastic modulus, which takes into account the internal fluid-pressure equilibration between two distinct porous phases.

The approach adopted in this study is to replace the heterogeneous porous media with effectively homogeneous porous media by reducing the internal local flow term. As a consequence, the effect of local flow is taken into account by a set of poroelastic parameters in the classical Biot theory. In other words, the resulting effectively homogeneous media is mathematically expressed in the form of classical Biot theory, but it actually incorporates the frequency dependent, wave-induced exchange of fluid fluxes between more compliant regions and relatively stiff regions. We call this effectively homogeneous porous media *effective Biot media*.

It is necessary to point out that the concept of effective Biot media is not limited to the DPDP model. It is also applicable to many other poroelastic models (Dutta and Odé, 1979a, 1979b; Dvorkin et al., 1995; Chapman et al., 2002; Müller and Gurevich, 2005; Carcione and Picotti, 2006; Yao et al., 2013), which can incorporate the effect of local flow into the corresponding effective poroelastic parameters, such as the effective drained bulk modulus, effective undrained bulk modulus, effective wavenumber, and so on. For example, rather than use the effective drained bulk modulus, Yao et al. (2013) propose to use the effective fluid modulus to account for the frequency-dependent internal flow effect. The geologic scenario can also be extended to the patchy-saturation model, squirt flow model, and others.

The importance of the concept of effective Biot media lies in that it allows for the local flow loss, but it does not require an analysis of a second slow wave. This is critical to the later treatment in this paper because the problem of solving the reflection coefficients from the boundary of heterogeneous porous media can be transformed to the problem of solving the reflection coefficients from the boundary of effective Biot media. Consequently, the problem of wave propagation characteristics and plane-wave boundary conditions can be cast in the framework of the classical Biot theory.

Phase velocities and attenuations

With all of the defined poroelastic parameters, the phase velocities and attenuations of effective Biot media can be determined. The wavenumber of the fast P-wave (k_{p1}), slow P-wave (k_{p2}), and S-wave (k_s) are, respectively, given by (Tang and Cheng, 2004)

$$\begin{aligned} k_{p1} &= k_{p0}\sqrt{\frac{1 + b_1\rho_f/\rho}{1 - b_1/b_0}}, \\ k_{p2} &= k_{p0}\sqrt{\frac{1 + b_2\rho_f/\rho}{1 - b_2/b_0}}, \\ k_s &= \omega\sqrt{\hat{\rho}/\mu^*}, \end{aligned} \tag{13}$$

where

$$\begin{aligned} b_1 &= \frac{1}{2}b_0\left[c - \sqrt{c^2 - 4\alpha(1-c)/b_0}\right], \\ b_2 &= \frac{1}{2}b_0\left[c + \sqrt{c^2 - 4\alpha(1-c)/b_0}\right], \\ b_0 &= M^*(K_u^* + 4\mu^*/3)/\alpha^*, \\ k_{p0} &= \omega/\sqrt{(K_u^* + 4\mu^*/3)/\rho}, \\ c &= (\alpha^* - b_s\rho/\rho_f b_0)/(\alpha^* + b_s), \\ b_s &= \rho_f\theta\omega^2, \hat{\rho} = \rho + \rho_f^2\omega^2\theta, \theta = i\kappa(\omega)/\eta\omega. \end{aligned} \tag{14}$$

Here, ρ and ρ_f are the bulk density and pore fluid density, respectively; μ^* is the effective undrained shear modulus, which is considered to be equal to dry rock's shear modulus μ_d; $\alpha^* = 1 - K_d^*/K_s$ is the effective frequency-dependent Biot's coefficient; $M^* = (\frac{\alpha^* - \phi}{K_s} + \frac{\phi}{K_f})^{-1}$, in which ϕ, K_f, and K_s are the porosity, fluid bulk modulus, and solid bulk modulus, respectively; and $\kappa(\omega)$ represents the overall dynamic permeability of the double-porosity composite and can be approximated using the harmonic average (Pride et al., 2004):

$$\frac{1}{\kappa(\omega)} = \frac{\nu_1}{\kappa_1(\omega)} + \frac{\nu_2}{\kappa_2(w)}, \tag{15}$$

where $\kappa_1(\omega)$ and $\kappa_2(\omega)$ are the dynamic permeability of the porous phases 1 and 2, respectively. The dynamic permeability for each phase is given as (Johnson et al., 1987)

Downloaded 04/06/15 to 112.10.114.108. Redistribution subject to SEG license or copyright; see Terms of Use at http://library.seg.org/

$$\kappa_i(\omega) = \frac{\kappa_i}{\left[1 - \frac{i}{2}\tau\kappa_i\rho_f\omega/(\eta\phi)\right]^{1/2} - i\tau\kappa_i\rho_f\omega/(\eta\phi)} (i = 1,2), \tag{16}$$

in which τ is the tortuosity and $\kappa_i (i = 1,2)$ are the previously mentioned static permeability of the phases 1 and 2, respectively.

Therefore, based on the wavenumbers computed in equation 13, the phase velocities of the fast P-wave (V_{P1}), slow P-wave (V_{P2}), and S-wave (V_{S}) are respectively calculated using

$$\begin{aligned} V_{\mathrm{P1}} &= \omega/\mathrm{Re}\{k_{p1}\}, \\ V_{\mathrm{P2}} &= \omega/\mathrm{Re}\{k_{p2}\}, \\ V_{\mathrm{S}} &= \omega/\mathrm{Re}\{k_s\}. \end{aligned} \tag{17}$$

Correspondingly, the attenuation of the fast P-wave (Qp_1^{-1}), slow P-wave (Qp_2^{-1}), and S-wave (Qs^{-1}) are given by

$$\begin{aligned} Qp_1^{-1} &= 2\,\mathrm{Im}\{k_{p1}\}/\mathrm{Re}\{k_{p1}\}, \\ Qp_2^{-1} &= 2\,\mathrm{Im}\{k_{p2}\}/\mathrm{Re}\{k_{p2}\}, \\ Qs^{-1} &= 2\,\mathrm{Im}\{k_s\}/\mathrm{Re}\{k_s\}, \end{aligned} \tag{18}$$

where $\mathrm{Re}\{k\}$ and $\mathrm{Im}\{k\}$ indicate the real and imaginary part of the wavenumber k, respectively.

Poroelastic reflection coefficients

We consider the poroelastic interface separating two effective Biot media denoted by superscripts 1 and 2, respectively, as shown in Figure 1. The incident wave is taken to be a fast P-wave of angular frequency ω, with an incident angle θ^i with respect to the normal to the boundary. At the interface, the incident wave is reflected into medium 1 and transmitted into medium 2, and in media the fast P-wave, slow P-wave, and SV-wave are generated.

To solve the seismic reflection and transmission at the interface of effective Biot medium, we have the boundary conditions (Deresiewicz and Rice, 1960; Dutta and Odé, 1983; Bourbié et al., 1987; Dai and Kuang, 2006) as follows:

1) continuity of the horizontal solid matrix displacement

$$u_x^1 = u_x^2 \tag{19}$$

2) continuity of the normal solid matrix displacement

$$u_z^1 = u_z^2 \tag{20}$$

3) continuity of the total normal stress

$$\sigma_{zz}^1 = \sigma_{zz}^2 \tag{21}$$

4) continuity of the total shear stress

$$\sigma_{xz}^1 = \sigma_{xz}^2 \tag{22}$$

5) continuity of the increment of fluid content

$$W_z^1 = W_z^2 \tag{23}$$

6) continuity of the fluid pressure

$$p_f^1 = p_f^2. \tag{24}$$

Note that the above boundary conditions are restricted to the $x - z$ plane, and they are only valid at the open-pore interface. Because the dynamic interaction between the upper and lower poroelastic media is frequency dependent, all those boundary conditions are hence also frequency dependent. The seismic reflection coefficients can therefore be calculated through solving the Zoeppritz-style equations:

$$GR = P, \tag{25}$$

where R is a 6×1 vector of the unknown reflection and transmission coefficients and is given by

$$R = \begin{pmatrix} R_{P1P1} \\ R_{P1P2} \\ R_{P1\,S} \\ T_{P1P1} \\ T_{P1P2} \\ T_{P1\,S} \end{pmatrix}. \tag{26}$$

Here, R_{P1P1}, R_{P1P2}, and $R_{P1\,S}$ are the reflection coefficients of the fast P-, slow P- and S-waves, respectively; T_{P1P1}, T_{P1P2}, and $T_{P1\,S}$ are the transmission coefficients of the fast P-, slow P- and S-waves, respectively; and G is a 6×6 matrix, which characterizes the angle-dependent dynamic poroelastic responses in the upper and lower half space of the effective Biot media:

$$\mathrm{G} = \begin{pmatrix} \sin\theta_{p1}^r & \sin\theta_{p2}^r & \cos\theta_s^r & -\sin\theta_{p1}^t & -\sin\theta_{p2}^t & \cos\theta_s^t \\ \cos\theta_{p1}^r & \cos\theta_{p2}^r & -\sin\theta_s^r & \cos\theta_{p1}^t & \cos\theta_{p2}^t & \sin\theta_s^t \\ X_1 & X_2 & X_3 & X_4 & X_5 & X_6 \\ \frac{\mu_1^*\sin 2\theta_{p1}^r}{V_{\mathrm{P}_{11}}} & \frac{\mu_1^*\sin 2\theta_{p2}^r}{V_{\mathrm{P}_{12}}} & \frac{\mu_1^*\cos 2\theta_s^r}{V_{\mathrm{S1}}} & \frac{\mu_2^*\sin 2\theta_{p1}^t}{V_{\mathrm{P}_{21}}} & \frac{\mu_2^*\sin 2\theta_{p2}^t}{V_{\mathrm{P}_{22}}} & -\frac{\mu_2^*\cos 2\theta_s^t}{V_{\mathrm{S2}}} \\ \delta_{p11}\cos\theta_{p1}^r & \delta_{p12}\cos\theta_{p2}^r & -\delta_{s1}\sin\theta_s^r & \delta_{p21}\cos\theta_{p1}^t & \delta_{p22}\cos\theta_{p2}^t & \delta_{s2}\sin\theta_s^t \\ \frac{\alpha_1^* M_1^* + M_1^*\delta_{p11}}{V_{\mathrm{P}_{11}}} & \frac{\alpha_1^* M_1^* + M_1^*\delta_{p12}}{V_{\mathrm{P}_{12}}} & 0 & -\frac{\alpha_2^* M_2^* + M_2^*\delta_{p21}}{V_{\mathrm{P}_{21}}} & -\frac{\alpha_2^* M_2^* + M_2^*\delta_{p22}}{V_{\mathrm{P}_{22}}} & 0 \end{pmatrix}, \tag{27}$$

where

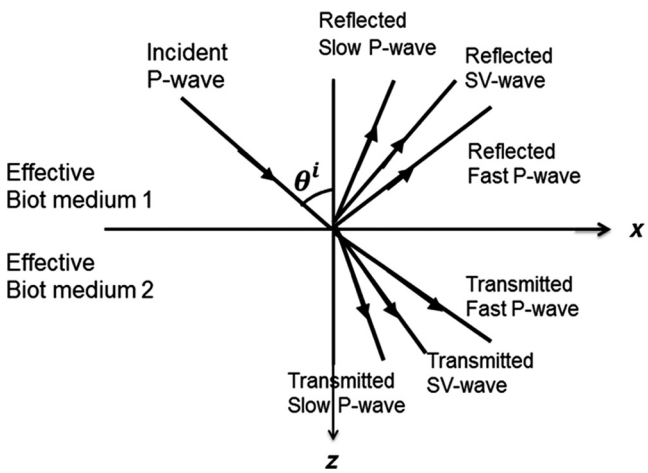

Figure 1. Reflection and transmission of a compressional plane wave at an interface between two effective Biot media. The effective single-porosity Biot medium is reduced from the double-porosity medium.

Downloaded 04/06/15 to 112.10.114.108. Redistribution subject to SEG license or copyright; see Terms of Use at http://library.seg.org/

$$X_1 = \frac{\lambda_1^* + (\alpha_1^*)^2 M_1^* + \alpha_1^* M_1^* \delta_{p11} + 2\mu_1^* (\cos\,\theta_{p1}^r)^2}{V_{\mathrm{P}_{11}}},$$
$$X_2 = \frac{\lambda_1^* + (\alpha_1^*)^2 M_1^* + \alpha_1^* M_1^* \delta_{p12} + 2\mu_1^* (\cos\,\theta_{p2}^r)^2}{V_{\mathrm{P}_{12}}},$$
$$X_3 = -\frac{2\mu_1^* (\cos\,\theta_s^r)^2}{V_{\mathrm{S1}}},$$
$$X_4 = -\frac{\lambda_2^* + (\alpha_2^*)^2 M_2^* + \alpha_2^* M_2^* \delta_{p12} + 2\mu_2^* (\cos\,\theta_{p1}^t)^2}{V_{\mathrm{P}_{21}}},$$
$$X_5 = -\frac{\lambda_2^* + (\alpha_2^*)^2 M_2^* + \alpha_2^* M_2^* \delta_{p12} + 2\mu_2^* (\cos\,\theta_{p2}^t)^2}{V_{\mathrm{P}_{22}}},$$
$$X_6 = -\frac{2\mu_2^* (\cos\,\theta_s^t)^2}{V_{\mathrm{S2}}}. \tag{28}$$

P is a 6×1 vector that represents the information of the incident P-wave in the upper medium and is given by

$$P = \begin{pmatrix} -\sin\,\theta^i \\ \cos\,\theta^i \\ X_7 \\ \frac{\mu_1^* \sin 2\theta^i}{V_{\mathrm{P}_{11}}} \\ \delta_{p11} \cos\,\theta^i \\ -\frac{\alpha_1^* M_1^* + M_1^* \delta_{p11}}{V_{\mathrm{P}_{11}}} \end{pmatrix}, \tag{29}$$

where $X_7 = -\frac{\lambda_1^* + (\alpha_1^*)^2 M_1^* + \alpha_1^* M_1^* \delta_{p11} + 2\mu_1^* (\cos\,\theta^i)^2}{V_{\mathrm{P}_{11}}}$.

Detailed derivations are carried out in Appendix A. In the above equations, $V_{\mathrm{P}_{11}}$, $V_{\mathrm{P}_{12}}$, V_{S1} and $V_{\mathrm{P}_{21}}$, $V_{\mathrm{P}_{22}}$, V_{S2} are the frequency-dependent fast P-wave velocity, slow P-wave velocity, and S-wave velocity in the upper medium and low medium, respectively, which can be calculated based on equation 17; $\lambda_i^* = K_{di}^* - \frac{2}{3}\mu_i^* (i = 1,2)$ is Lame's parameter of the effective Biot media under a drained condition; δ_{pi1}, δ_{pi2}, and $\delta_{si,}(i = 1,2)$ refer to the ratios of the potential for the relative fluid displacement to the rock frame displacement for the fast P-wave, slow P-wave, and S-wave, respectively; θ_{p1}^r, θ_{p2}^r, and θ_s^r refer to the reflected angles of the fast P-wave, slow P-wave, and S-wave, respectively; and θ_{p1}^t, θ_{p2}^t, and θ_s^t refer to the transmitted angles of the fast P-wave, slow P-wave, and S-wave, respectively.

Following Snell's law in effective Biot media (equation A-17 in Appendix A), they can be expressed as

$$\theta_{p1}^r = \theta^i, \quad \theta_{p2}^r = \arcsin\frac{\sin\,\theta^i}{V_{\mathrm{P11}}} V_{\mathrm{P12}},$$
$$\theta_s^r = \arcsin\frac{\sin\,\theta^i}{V_{\mathrm{P11}}} V_{\mathrm{S1}}, \quad \theta_{p1}^t = \arcsin\frac{\sin\,\theta^i}{V_{\mathrm{P11}}} V_{\mathrm{P21}}, \tag{30}$$
$$\theta_{p2}^t = \arcsin\frac{\sin\,\theta^i}{V_{\mathrm{P11}}} V_{\mathrm{P22}}, \quad \theta_s^t = \arcsin\frac{\sin\,\theta^i}{V_{\mathrm{P11}}} V_{\mathrm{S2}}.$$

The resulting reflection coefficients now become complex numbers due to the wave dispersion and attenuation in heterogeneous poroelastic media. Thus, we can define the reflection coefficients as

$$R(\omega) = |R(\omega)| \exp(i\varphi), \tag{31}$$

where $|R(\omega)|$ indicates the magnitude and φ indicates the phase angle for the poroelastic reflection coefficients. In the following sections, we will use these two parameters to characterize the reflection dispersion signatures. However, note that if the porosity ϕ in equation 25 goes to zero, the wave-induced fluid flow will naturally disappear. In this case, it is easy to demonstrate that equation 25 will be consequently reduced to the classical Zoeppritz equations.

It is necessary to point out that all of the frequency-dependent poroelastic parameters in equation 25 are computed based on the effective single-porosity Biot model reduced from the double-porosity model, which suggests that the effect of local flow is incorporated into the poroelastic wave propagation. Correspondingly, the resulting reflection coefficients will also contain the responses from Biot flow in combination with local flow.

A NUMERICAL EXAMPLE

So far, we have presented a theoretical formulation of the reflection and transmission of plane seismic waves at a boundary between two heterogeneous porous rocks. In this section, we use a numerical example to quantitatively investigate the impact of wave-induced fluid flow on the seismic reflection coefficients at a wide range of angles and frequencies.

Geologic model

We only consider an interface with two heterogeneous porous half-spaces above and below. To mimic the realistic reservoir situation, we assume that the geologic model consists of an underlain sandstone reservoir with an overburden shale layer. The sandstone and shale have heterogeneous porous structures, which can be characterized by the double-porosity model. To obtain their elastic properties, we start with a solid rock matrix, in which the minerals are mixed using a Voigt-Reuss-Hill average (Mavko et al., 2009). The mineral presenting in the upper medium (shale) consists of 85% clay and 15% feldspar. The mineral presenting in the lower medium (sandstone) consists of 95% quartz and 5% clay, implying that the sandstone is pretty clean. The heterogeneity phases (phase 2) in the sandstone and shale are assumed to represent the compliant parts of the rock, whereas the matrix phases (phase 1) are considered to be well consolidated.

Matrix rock properties for the overburden shale and underlain sandstone are given in Table 1, where K_s and μ_s are the bulk and shear moduli for the mineral matrix; K_d and μ_d are the bulk and shear moduli of the dry rock frame; ϕ is the porosity, and note that the porosities in the shale represent effective porosity, which can be considered to get involved in the wave-induced fluid flow; τ is the tortuosity parameter; and v indicates the volume fraction of phase 1 or 2. The geometry of the heterogeneity phase is assumed as penny shaped, and α and ε are used to represent the radius and aspect ratio of the heterogeneity, respectively. Two geometric parameters L_1 and V/S can be hence calculated using α and ε (Pride et al., 2004). The properties of fluids are listed in Table 2, where K_f, ρ_f, and η are the bulk modulus, density, and viscosity of the pore fluid, respectively. The overburden shale is assumed to be brine saturated with viscosity of 1 cP, and the underlain sandstone is assumed to be oil saturated with viscosity of 5 cP. Here, we only investigate the situation of fully saturated reservoir rocks. Note that the wave dispersion and attenuation caused by heterogeneous saturation in partially saturated reservoir rocks, where fluids exchange between

Downloaded 04/06/15 to 112.10.114.108. Redistribution subject to SEG license or copyright; see Terms of Use at http://library.seg.org/

patches of different fluids, are not considered in this study. Also, for simplicity, we assume that the host phase and heterogeneous phase have the same mineral composition, but with a different level of consolidation. The dry rock moduli are determined from the following effective medium formula (Walton, 1987; Pride et al., 2002; Pride and Berryman, 2003a):

$$K_d^i = (1-\phi_i)K_s/(1+c_i\phi_i),$$
$$\mu_d^i = (1-\phi_i)\mu_s/(1+c_i\phi_i), \tag{32}$$

where we take $c_1 = 6$ and 4 for the well consolidated host phase and $c_2 = 180$ and 100 for the poorly consolidated heterogeneity phase, in sandstone and shale, respectively. The overall drained bulk modulus and shear modulus for the double-porosity composite are computed by harmonic average for the effective media. The harmonic average actually represents the isostress condition, which is considered to be reasonably representative to describe the overall elastic responses of the heterogeneous sedimentary rocks because the soft phases (heterogeneity) likely have a shape that is prone to be more elongated than compact (Pride et al., 2004). It should be emphasized that, if the real frame moduli are stiffer than those predicted by the harmonic average, the passing seismic wave will create less fluid pressure difference and hence reduce the amount of mesoscopic flow loss discussed here (Yao, 2013).

These frame moduli are substituted into equation 6 to obtain the constants a_{ij}; then, we can use equations 10–12 to compute the poroelastic moduli of effective Biot media; finally, with all those parameters for the given geologic model, the phase velocities and the reciprocal of the quality factors for the double-porosity composite are computed based on equations 17 and 18, respectively.

Velocity dispersion and attenuation characteristics

The fast P-wave velocities for the upper and lower media are plotted against frequency in Figure 2a. The solid lines represent the velocity dispersion calculated based on the effective Biot theory, which takes into account the effect of local flow and Biot flow. We observe considerable velocity dispersion for the heterogeneous sandstone at a low-frequency range of 10–100 Hz. By contrast, the overburden shale exhibits much less dispersion effects, and the transitional frequency occurs at very low frequency (less than 1 Hz). The mesoscopic flow is considered to be responsible for such dispersion effects. Moreover, there is a slight ramp-up in the fast P-wave for the upper medium and lower medium centered at a much higher frequency, which is considered to be caused by the Biot flow. Nevertheless, if we ignore the impact of local flow, as the dashed lines illustrate, the classical Biot theory only predicts a negligible dispersion effect. The attenuations of the fast P-wave for the upper and lower media are plotted against frequency in Figure 3a. The peak to the left for each attenuation curve corresponds to the frequency at which the mesoscopic heterogeneity structure just has time to equilibrate in one cycle, whereas the peak to the right corresponds to the Biot-loss maximum. Note that such a dependence of the characteristic frequency on rock and fluid properties (such as permeability and viscosity) for the mesoscopic fluid flow is opposite to that of the Biot flow. It is also easy to determine that the local viscous flow contributes to most of the dissipative energy in the low-frequency range, whereas the global Biot flow plays a dominant role in the energy dissipation for the high-frequency domain.

In Figures 2b and 3b, the slow P-wave exhibits fundamentally different physical behavior in comparison with the fast P-wave. At a lower frequency range, the velocity of the slow P-wave is very low, approximating to zero. It then ramps up to approximately 700 m/s at a higher frequency range. Attenuation of the slow P-wave is very high at a low frequency, and then it decreases significantly at a higher frequency. Although the slow P-wave only propagates a very short distance before being fully dissipated, the slow P-wave can markedly influence the fast P-wave reflection amplitudes, which commonly carry information about the porous media away from the interface to distant receivers. The S-wave dispersion and the corresponding $1/Q$ for the upper and lower media are plotted against frequency in Figures 2c and 3c, respectively. Compared with the fast P-wave dispersion and attenuation, the S-wave does not show a dispersion effect due to mesoscopic flow. Nonetheless, it is interesting to note that the S-wave dispersion and attenuation caused by Biot flow are larger than those of the corresponding fast P-wave dispersion.

Reflection dispersion signatures

For the given set of parameters, Figure 4 shows the computed reflection amplitude and phase variation of the fast PP-wave as a function of the frequency and incident angle. In the amplitude versus incident angle (AVA) domain, Figure 4a shows that the

Table 1. Related parameters for rock frame properties of the upper and lower media.

	Rock frame properties			
	Upper (shale)		Lower (sandstone)	
Parameter	Phase 1	Phase 2	Phase 1	Phase 2
K_d (GPa)	22.0	4.2	14.2	0.58
μ_d (GPa)	6.9	1.5	15.6	0.64
v	0.93	0.07	0.96	0.04
ϕ	0.05	0.06	0.25	0.30
κ (md)	0.01	100	10	1000
α (m)	—	0.05	—	0.08
ε	—	0.1	—	0.1
τ	2.4	2	2.4	2

Table 2. Related parameters for the pore fluid properties of the upper and lower media.

	Pore fluid properties	
Parameter	Upper (brine)	Lower (oil)
K_f (GPa)	3.0	2.1
ρ_f (g/cm^3)	1.05	0.94
η (cP)	1	5

Downloaded 04/06/15 to 112.10.114.108. Redistribution subject to SEG license or copyright; see Terms of Use at http://library.seg.org/

reflection magnitude increases with an increase of the incident angle, which agrees with the traditional class III AVO response (Rutherford and Williams, 1989). In the amplitude versus frequency domain, the low-frequency bright-spot channel occurring at the seismic frequency band is intimately associated with the physical discrepancy between the characteristic frequency of the overburden shale and underlain reservoir sandstone. In a general way, the AVA relationship is mainly influenced by the contrast of elastic properties, such as P-impedance and the V_P/V_S ratio. However, the amplitude versus frequency relationship contains information about the heterogeneities' properties and fluid mobility. Figure 4b shows the phase shift of the poroelastic reflection compared with that of elastic reflection. It is found that the phase variation is also dependent on the frequency and a nonnegligible phase shift, which can be as high

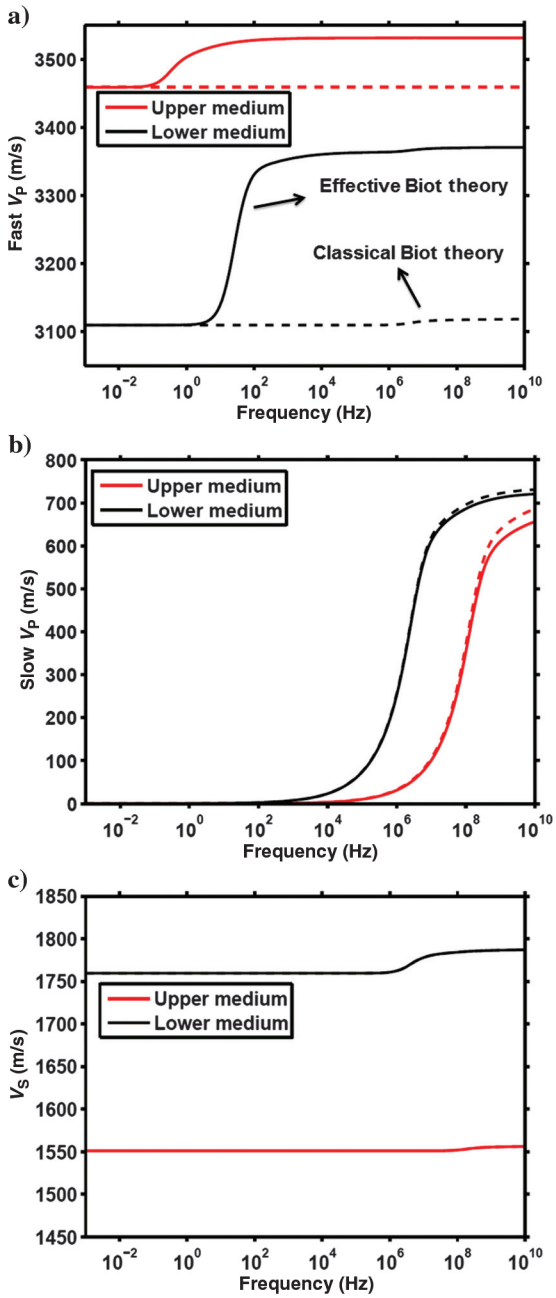

Figure 2. (a) Velocities of fast P-waves, (b) slow P-waves, and (c) S-waves with respect to the frequency in the upper and lower double-porosity medium (parameters are shown in Tables 1 and 2). The frequency range is from 10^{-3} to 10^{10} Hz, plotted on a logarithmic scale. To highlight the effect of local flow, the dashed lines represent the velocity dispersion predicted by classical Biot theory including only the effect of global Biot flow.

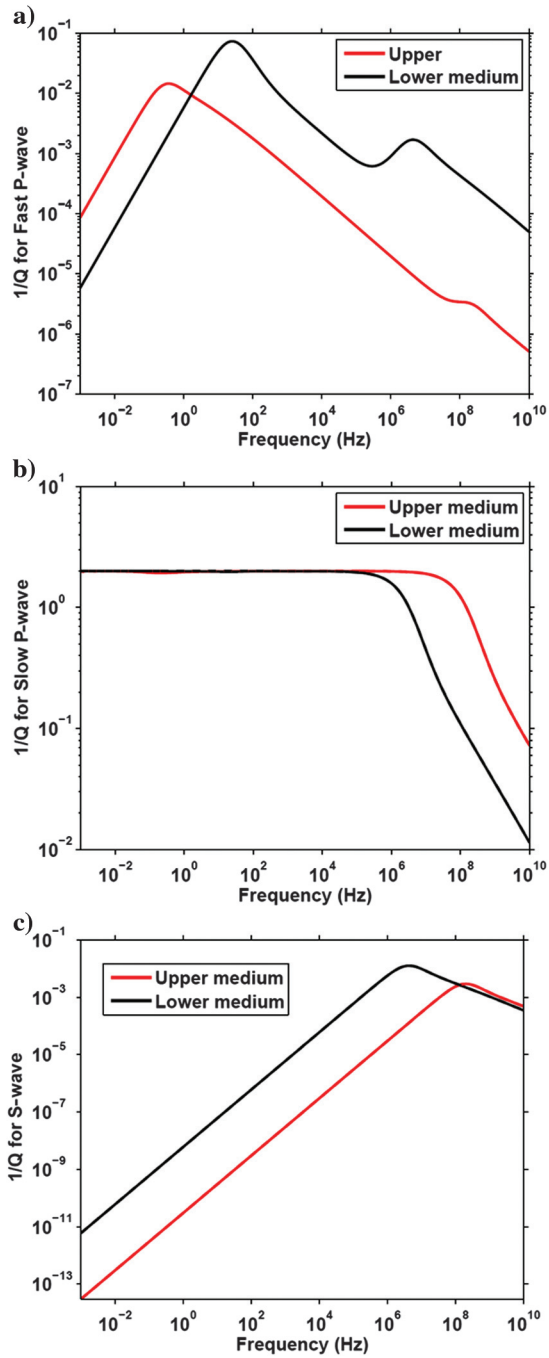

Figure 3. (a) Attenuation of fast P-waves, (b) slow P-waves, and (c) S-waves with respect to the frequency in the upper and lower double-porosity media (parameters in Tables 1 and 2). The frequency range is from 10^{-3} to 10^{10} Hz, plotted on a logarithmic scale.

Downloaded 04/06/15 to 112.10.114.108. Redistribution subject to SEG license or copyright; see Terms of Use at http://library.seg.org/

as 16°, occurs in the seismic exploration band. Nonetheless, the phase variation shows little sensitivity to the incident angle change.

Now, we are going to give a detailed analysis regarding the fast PP reflectivity dispersion characteristics (Figure 5) at a normal incident angle. For the purpose of comparison: The black solid lines indicate the heterogeneous poroelastic reflection including the effect of local mesoscopic flow and global Biot flow; the blue lines represent the poroelastic reflection, which only takes into consideration of global Biot flow; and the red dashed lines indicate the elastic reflection coefficient, which is computed from the classical Zoeppritz equation (Aki and Richards, 1980). Correspondingly, in the case of elastic reflection, the saturated rock's elastic responses are computed using the Gassmann (1951) equation, which suggests that the reflection coefficients do not include any intrinsic dispersion effects. As we can observe in Figure 5a, the elastic reflection is consistent with the Biot reflection and the heterogeneous poroelastic reflection only at a frequency band as low as 10^{-2} Hz. Such a consistency physically makes sense because the global Biot flow becomes negligible at a very low frequency, and the local mesoscopic flow does not induce a dispersion effect at very low frequency. It can be concluded that the porous dissipative medium acts as an elastic medium only at a very low frequency ($<10^{-2}$ Hz). Regarding the dispersion characteristic of the heterogeneous poroelastic reflection, the reflectivity dispersion occurring at roughly 0.01–100 Hz is evidently caused by mesoscopic flow, and the maximum dispersion effect at the seismic frequency domain can reach as high as 40%. This huge dispersion effect should not be ignored when using seismic reflections for quantitative seismic interpretation. Moreover, the negligible reflectivity dispersion occurring above 10^6 Hz (the ultrasonic lab frequency band) is evidently associated with Biot flow.

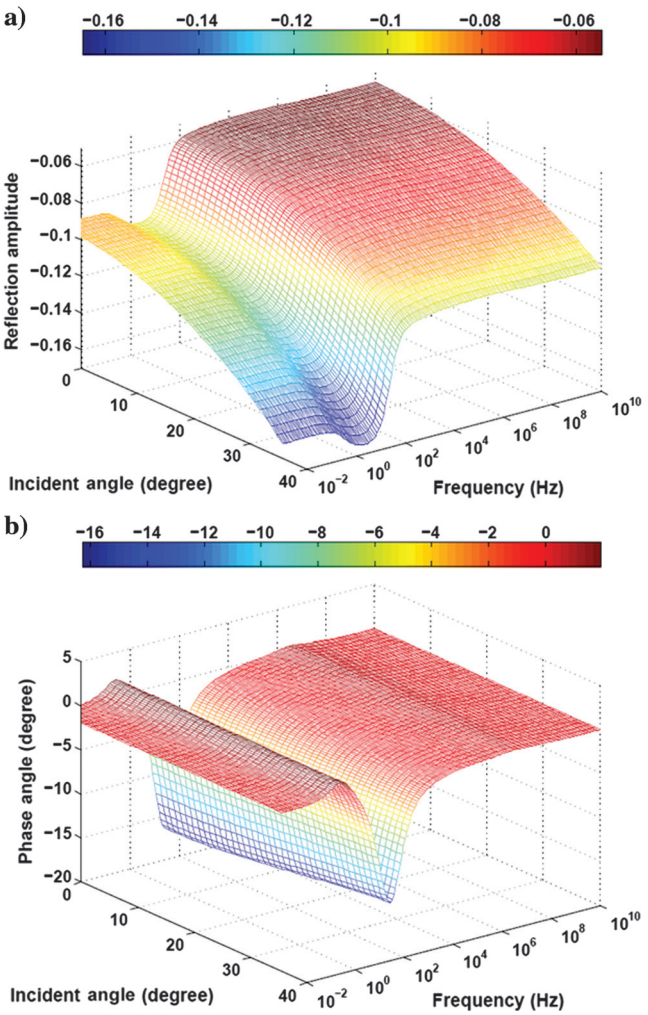

Figure 4. (a) Reflection amplitude and (b) phase variation of the fast PP wave as a function of frequency and incidence angle. Here, phase variation indicates the deviation of the phase in the poroelastic reflection from the constant phase in the elastic reflection.

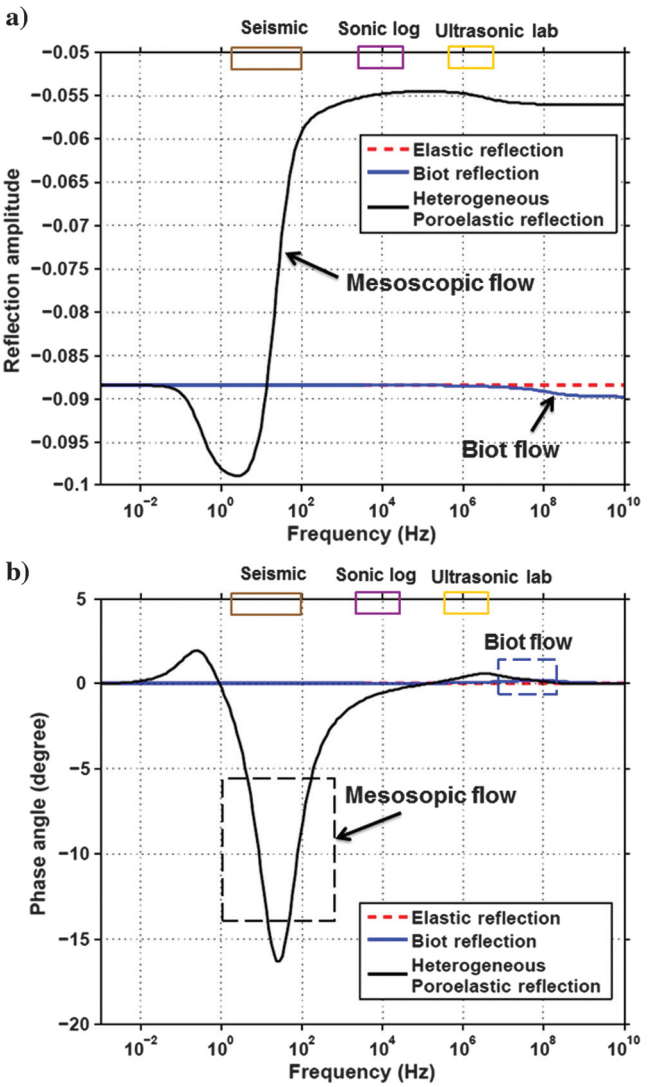

Figure 5. Reflection (a) amplitude and (b) phase of the fast PP wave as a function of frequency at a normal incidence angle. The red dashed lines indicate the reflection coefficients computed for elastic reflection, the blue solid lines indicate reflection coefficients computed using the classical Biot theory, and the black solid lines indicate the heterogeneous poroelastic reflection including the effect of local mesoscopic flow and global Biot flow. The frequency bands for the seismic, VSP, sonic log, and ultrasonic lab are highlighted in the plot.

Downloaded 04/06/15 to 112.10.114.108. Redistribution subject to SEG license or copyright; see Terms of Use at http://library.seg.org/

Figure 5b plots the phase variation against the frequency at a normal incident angle. The phase angle of the poroelastic reflection is consistent with that of the elastic reflection at the low- and high-frequency limits. A phase advance occurs at 10^{-3} to approximately 10^{-1} Hz, but then a noticeable phase delay takes place at a broad frequency range from 10^{-1} to 10^{5} Hz. Both of these phase shifts are mainly caused by the local mesoscopic flow. The small phase advance occurring above 10^{6} Hz is considered to be closely related to the dispersion caused by the Biot flow.

Figure 6 shows the converted PS reflection as a function of frequency. PS reflectivity is zero at a normal incident angle, which is physically understandable because no PS conversion occurs at a normal incident angle. At a nonzero incident angle, we observe that the PS reflection presents a similar dispersion trend to what the fast PP reflectivity does. However, it should be noted that the relative dispersion effect for the PS reflection is bigger than that of the fast PP reflection. In particular, the dispersion effect due to Biot flow is more evident. Additionally, we find that the PS reflection has a larger dispersion effect for the far offset than the near offset for the given geologic model.

Implications for reservoir characterization

Figure 7 shows the AVO relationship with different frequencies in the seismic exploration band. One valuable feature we can observe from the angle- and frequency-dependent amplitude is that the AVO intercept and gradient (Castagna et al., 1998) are strongly impacted by wave-induced fluid flow. Obviously, neglecting the dispersion behavior of the reflectivity will bias the interpretation of AVO signatures. For example, because the amplitude of reflectivity might be considerably diminished due to dispersion behavior caused by local flow, the class III AVO response can be possibly interpreted as a class II AVO response (Rutherford and Williams, 1989) by mistake. Note that those observations are based on the assumption that the frequency contents are the same at all angles of incidence. Nonetheless, in practice, many other factors can also affect the seismic frequency contents in the offset domain. For example, wavelet stretching due to NMO correction often causes the loss of high frequency for far-offset seismic data.

For the purpose of reservoir evaluation, it is a common practice to use the seismic reflection amplitude to estimate porosity, water saturation, or other reservoir properties. Be aware that the field reflection observations, which are often centered approximately 40–60 Hz, already represent the reflection dispersion effect. That is to say, in heterogeneous reservoir rocks, the classical seismic reflection interpretation based on the classical Zoeppritz equation and Gassmann fluid substitution might be misleading. For example, for the given geologic model, if we use the dispersive seismic reflection amplitude to predict porosity, the result will be considerably underestimated. Consequently, the quantification of the poroelastic impact on seismic analysis can provide insights to improve quantitative reservoir characterization.

Note that the mesoscopic flow also influences the phase angle to a considerable degree, and it consequently affects the seismic waveform. This implies that a phase shift caused by reflection dispersion can lead to uncertainty for seismically imaging the precise location of the geologic feature of interest. In addition, as illustrated in Figure 5, the significant discrepancy of the seismic amplitude and phase variation between the surface seismic band and the sonic log band also suggests that we should be more cautious about the seismic-to-synthetic well tie in heterogeneous reservoir rocks.

DISCUSSIONS

Equation 25 presents poroelastic Zoeppritz-style reflectivity incorporating the effect of wave-induced fluid flow. It is important to realize the physically distinctive differences between this equation and the classical Zoeppritz equation. Theoretically, the classical Zoeppritz equation is not applicable for calculating the reflection coefficients in heterogeneous and dissipative media because the

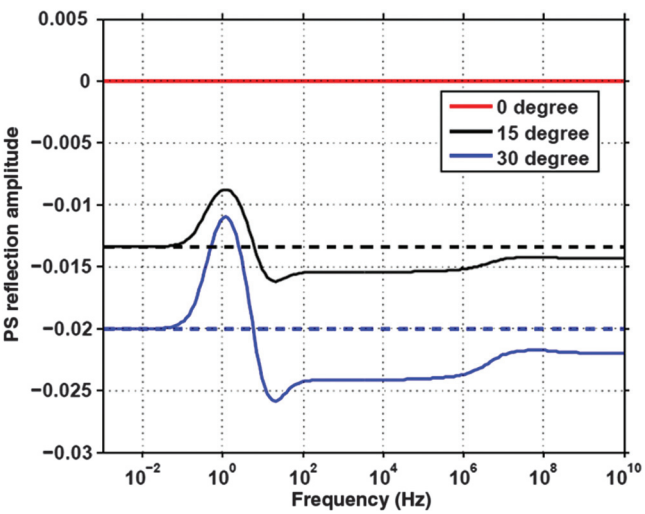

Figure 6. Comparisons of PS reflectivity dispersion at incident angles of 0°, 15°, and 30°. The dashed line indicates the PS reflection coefficients computed based on the Zoeppritz equation.

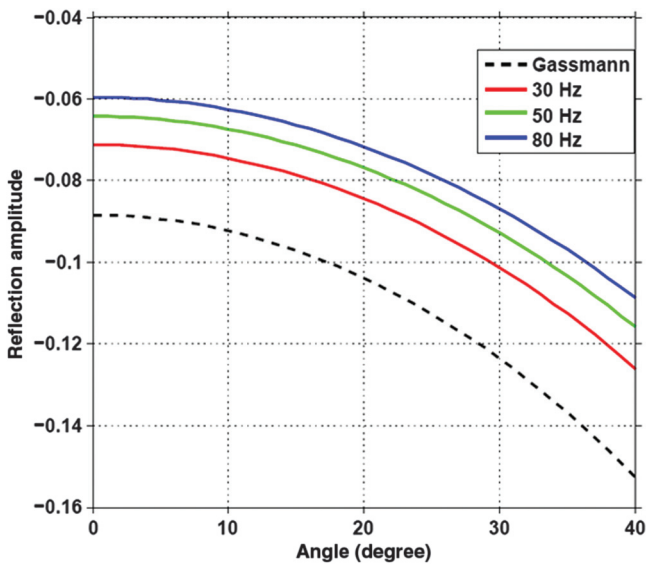

Figure 7. AVO relationship with a different frequency in the seismic band. The central frequency band for the field observation is often centered at approximately 40–60 Hz. The black dashed line indicates the reflection computed from the Zoeppritz equation, which often represents the low-frequency limit for the poroelastic reflection.

Downloaded 04/06/15 to 112.10.114.108. Redistribution subject to SEG license or copyright; see Terms of Use at http://library.seg.org/

well-known assumption for the Zoeppritz equation is that the medium is elastic and nondissipative (Aki and Richards, 1980). From the perspective of energy conservation, the classical Zoeppritz equation only takes into account the conservation of elastic energy. To be specific, the total energy of particle motion, including the volume of integral of kinetic energy and elastic strain energy throughout the elastic medium, has been held constant (Aki and Richards, 1980). However, the "poroelastic" Zoeppritz equation not only includes the elastic energy but also the dissipative energy, which comes from the pore pressure diffusion caused by Biot flow and local viscous flow. Moreover, the reflection calculated based on the classical Zoeppritz equation cannot give the phase variation with frequency, which however is an inseparable part of the poroelastic reflection feature.

It is also necessary to point out that the methodology to compute poroelastic reflection coefficient here is distinct from the derivation of reflection coefficients in viscoelastic media (White, 1965; Bourbié, 1983; Lines et al., 2008; Quintal et al., 2009; Ren et al., 2009; Liu et al., 2011; Morozov, 2011). Even though the velocity and attenuation inputs in their methods are considered as frequency dependent, the dynamic interactions regarding the fluid flow between the upper and lower poroelastic medium are ignored. However, in our study, the continuity of the increments of fluid content and fluid pressure in equation 19 explicitly takes into account the dynamic interaction between the upper and lower heterogeneous poroelastic medium.

It is well known that AVO gradient information is strongly dependent on the V_P/V_S ratio. Therefore, S-wave dispersion characteristics play an important role in understanding frequency-dependent AVO signatures. S-wave dispersion caused by Biot flow can be calculated on the basis of Biot's poroelastic wave propagation method (Biot, 1956a, 1956b, 1962). Despite the fact that S-wave dispersion and attenuation due to local flow have been experimentally observed (Adam et al., 2006; Batzle et al., 2006) and numerically simulated (Masson and Pride, 2007; Rubino et al., 2009; Wenzlau et al., 2010; Quintal et al., 2012), the physical mechanisms standing behind those observations have not been fully understood yet. Many poroelastic models have been proposed to quantify P-wave attenuation in fully saturated elastically heterogeneous or partially saturated media (White, 1975; Dutta and Odé, 1979a, 1979b; Gelinsky and Shapiro, 1997; Gurevich et al., 1997; Shapiro and Müller, 1999; Pride and Berryman, 2003a, 2003b; Müller and Gurevich, 2004, 2005; Carcione and Picotti, 2006; Müller et al., 2007); however, no analytical solution concerning the S-wave attenuation due to local flow is developed. In this study, S-wave dispersion due to mesoscopic flow is ignored. To fully characterize the angle and frequency-dependent reflectivity, especially the associated AVO signatures, an accurate description of S-wave dispersion in a heterogeneous porous composite should be investigated in the future.

The double-porosity model we used here is based on the idealization that heterogeneous porous media can be meaningfully reduced to just two distinct porous phases with a single dominant diffusion length and contrasting properties. The idealization of the model may limit its application on some complex heterogeneous reservoirs, which often involves mixing many porous phases and multiscale heterogeneities in a random manner. Also, to generate the effective Biot media from the double-porosity model, heterogeneity phase 2 is assumed entirely embedded in host phase 1. This implies that the volume fraction of phase 2 is much smaller compared with that of phase 1, which may not meet the conditions of real rocks in some geologic scenarios. Besides, in the numerical example, we assume the geometry of the heterogeneity phase is ellipsoidal. This is for the sake of simplicity because in real sedimentary rocks, the heterogeneities often exhibit an extremely complex and irregular shape. However, the real challenge concerning the practical implementation of this methodology is the difficulty in prescribing appropriate physical parameters, such as heterogeneity size, tortuosity, and bulk modulus in the drained condition.

Similar to any other sedimentary rocks, shales more or less contain heterogeneities to some extent. Such heterogeneities often come from the presence of microcracks or organic material related to hydrocarbon generation (Vernik, 1994), compositional variation due to different depositional environments, and so forth. As a consequence, shales are naturally dispersive materials, even though they might behave elastically in seismic exploration band due to their very low permeability characteristics (Batzle et al., 2006). To investigate the frequency-dependent reflection variations due to patchy-saturated rocks, Ren et al. (2009) and Liu et al. (2011) assume that the overlying shale is nondispersive. However, in this study, to preserve the generality of poroelastic reflection in heterogeneous poroelastic media, the overburden shale is considered as a dispersive medium including mesoscopic heterogeneity. Even the dispersion effect is not appreciable, and it occurs in a very low frequency domain, as we can see in Figures 2 and 3. The permeability of shale in our designed geologic model is given as 0.01 md, but the permeability of shales can vary enormously, from the nanodarcy to the microdarcy range. Figure 8 illustrates how the permeability of the overburden shale influences the reflection amplitude. It turns out that the reflection dispersion curve merely shows a noticeable change at the low-frequency domain (<10 Hz), with the seismic amplitude getting stronger as the permeability of the overburden shale decreases.

Finally, the present study focuses on theoretical modeling. Conclusive evidence for reflection dispersion due to wave-induced fluid flow from lab measurements and field observations is still lacking.

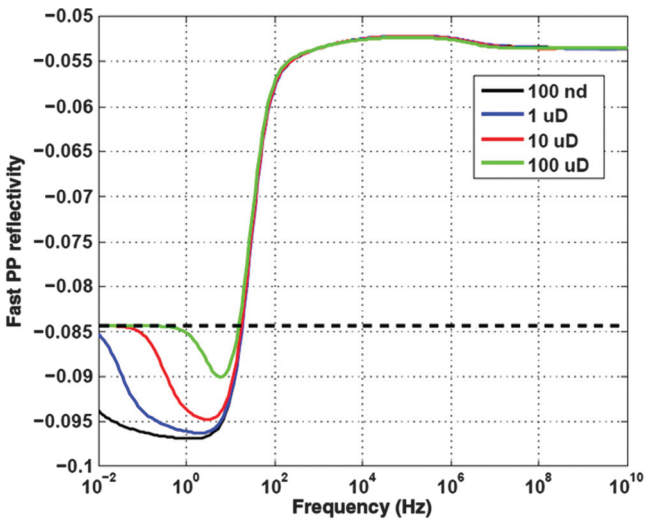

Figure 8. The effect of permeability of overburden shale on PP reflection dispersion at a normal incident angle. The dashed line indicates PP reflection coefficients computed based on the Zoeppritz equation.

Downloaded 04/06/15 to 112.10.114.108. Redistribution subject to SEG license or copyright; see Terms of Use at http://library.seg.org/

On the one hand, this is due to the difficulty in making appropriate measurements. On the other hand, the observed field seismic reflections may include the contribution of intrinsic attenuation and scattering attenuation due to the presence of extensive heterogeneities. At the present time, techniques that can reliably separate the total inferred loss into scattering and intrinsic portions are generally not available (Pride et al., 2004).

CONCLUSIONS

In the present work, we have quantified the impact of mesoscopic flow and Biot flow simultaneously on the seismic reflection at the interface between two heterogeneous porous media. For a typical reflection interface of heterogeneous porous sandstone overlain by shale, with the relevant physical parameters used in the numerical modeling, it is found that (1) wave-induced fluid flow makes the seismic amplitude and phase angle become frequency- and angle-dependent, which not only depends on the elastic properties contrast, but also strongly relies on the fluid mobility and heterogeneity features, (2) the poroelastic reflections are identical to the elastic reflection at the low-frequency limit. However, this only takes place at frequency ranges below 10^{-2} Hz, (3) at the seismic exploration band, the variation of seismic amplitude caused by local mesoscopic flow is approximately 40%, and a noticeable phase shift (16°) is also produced, and (4) the global Biot flow effect on reflectivity is almost trivial and occurs mainly above the ultrasonic frequency band.

Reflection dispersion effects due to mesoscopic flow cannot be ignored because the classical quantitative seismic interpretation might be misleading. Also, the phase variation caused by local flow can bring uncertainty for seismically imaging the geologic structure. Additionally, for a wide frequency range, the significant discrepancy of the seismic amplitude and phase variation at surface seismic, VSP, and sonic log frequency bands also suggests that we should be more cautious about the full integration of geophysical measurements at various scales in heterogeneous reservoir rocks. The implications of reflection dispersion for characterization of heterogeneous reservoirs rocks are encouraging, which leaves open the possibility of using frequency-dependent seismic attributes to decipher geologic heterogeneity features and fluid mobility characteristics.

ACKNOWLEDGEMENT

This work was sponsored by the Fluids and DHI Consortium of the Colorado School of Mines and the University of Houston. Special thanks also go to J. Castagna and L. Thomsen for the illuminating discussions on this topic.

APPENDIX A

SEISMIC REFLECTION COEFFICIENTS FROM THE BOUNDARY OF EFFECTIVE BIOT MEDIA

To facilitate computations, we consider Helmholtz decomposition of the two displacement vectors **u** and **W** in the form

$$\begin{cases} \mathbf{u} = \nabla\varphi_s + \nabla\times\psi_s, \\ \mathbf{W} = \nabla\varphi_f + \nabla\times\psi_f, \end{cases} \tag{A-1}$$

where φ_s and ψ_s are the potential functions associated with the displacement vectors of the rock frame and φ_f and ψ_f are the potential functions associated with the displacement vectors of fluid with respect to the solid frame.

Because the geometry is illustrated in Figure 1, we consider the seismic reflections at the interface of two effective Biot media. For 2D plane-wave propagation, the displacement potentials of the incident, reflected, and transmitted waves can be written in the form

$$\text{incident P}-\text{wave}: \begin{cases} \varphi_s^i = A_{s1}^i e^{ik_{p1}^i(\sin\theta^i x+\cos\theta^i z)-i\omega t}, \\ \varphi_f^i = A_{f1}^i e^{ik_{p1}^i(\sin\theta^i x+\cos\theta^i z)-i\omega t}, \end{cases} \tag{A-2}$$

reflected SV−wave:

$$\begin{cases} \varphi_s^r=\varphi_{s1}^r+\varphi_{s2}^r=A_{s1}^r e^{ik_{p1}^r(\sin\theta_{p1}^r x-\cos\theta_{p1}^r z)-i\omega t}+A_{s2}^r e^{ik_{p2}^r(\sin\theta_{p2}^r x-\cos\theta_{p2}^r z)-i\omega t}, \\ \varphi_f^r=\varphi_{f1}^r+\varphi_{f2}^r=A_{f1}^r e^{ik_{p1}^r(\sin\theta_{p1}^r x-\cos\theta_{p1}^r z)-i\omega t}+A_{f2}^r e^{i\omega t-ik_{p2}^r(\sin\theta_{p2}^r x-\cos\theta_{p2}^r z)-i\omega t}, \end{cases} \tag{A-3}$$

$$\text{reflected SV}-\text{wave}: \begin{cases} \psi_s^r = B_s^r e^{ik_s^r(\sin\theta_s^r x-\cos\theta_s^r z)-i\omega t}, \\ \psi_f^r = B_f^r e^{ik_s^r(\sin\theta_s^r x-\cos\theta_s^r z)-i\omega t}, \end{cases} \tag{A-4}$$

transmitted P−wave:

$$\begin{cases} \varphi_s^t=\varphi_{s1}^t+\varphi_{s2}^t=A_{s1}^t e^{ik_{p1}^t(\sin\theta_{p1}^t x+\cos\theta_{p1}^t z)-i\omega t}+A_{s2}^t e^{ik_{p2}^t(\sin\theta_{p2}^t x+\cos\theta_{p2}^t z)-i\omega t}, \\ \varphi_f^r=\varphi_{f1}^t+\varphi_{f2}^t=A_{f1}^t e^{ik_{p1}^t(\sin\theta_{p1}^t x+\cos\theta_{p1}^t z)-i\omega t}+A_{f2}^t e^{ik_{p2}^t(\sin\theta_{p2}^t x+\cos\theta_{p2}^t z)-i\omega t}, \end{cases} \tag{A-5}$$

$$\text{transmitted SV}-\text{wave}: \begin{cases} \psi_s^t = B_s^t e^{ik_s^t(\sin\theta_s^t x+\cos\theta_s^t z)-i\omega t}, \\ \psi_f^t = B_f^t e^{ik_s^t(\sin\theta_s^t x+\cos\theta_s^t z)-i\omega t}, \end{cases} \tag{A-6}$$

where the superscripts i, r, and t denote the incident, reflection, and transmission waves, respectively; k_{p1}^i is the wavenumber of the incident fast P-wave; k_{p1}^r, k_{p2}^r, and k_s^r are the wavenumbers of two reflected P- and reflected S-waves in the effective Biot medium 1, respectively; k_{p1}^t, k_{p2}^t, and k_s^t are the wavenumbers of two transmitted P- and transmitted S-waves in the effective Biot medium 2, respectively; $A_{s1}^m (m = i, r, t)$ and A_{f1}^m denote, respectively, the potential amplitude of the fast P-wave associated with the displacement of the rock frame and relative fluid flow; $A_{s2}^m (m = i, r, t)$ and A_{f2}^m denote, respectively, the potential amplitude of the second P-wave associated with the displacement of the rock frame and relative fluid flow; $B_s^m (m = r, t)$ and B_f^m denote, respectively, the potential amplitude of the S-wave associated with the displacement of the rock frame and relative fluid flow.

Following the earlier work by Deresiewicz and Rice (1960), Dutta and Odé (1983), and Dai and Kuang (2006), the potential of the rock frame displacement is related to that of the relative fluid flow displacement by a constant. Therefore, we have such a relationship for medium 1

$$\frac{A_{f1}^i}{A_{s1}^i} = \delta_{p11}, \quad \frac{A_{f1}^r}{A_{s1}^r} = \delta_{p11}, \quad \frac{A_{f2}^r}{A_{s2}^r} = \delta_{p12}, \quad \text{and} \quad \frac{B_f^r}{B_s^r} = \delta_{s1}; \tag{A-7}$$

Downloaded 04/06/15 to 112.10.114.108. Redistribution subject to SEG license or copyright; see Terms of Use at http://library.seg.org/

and similarly, for medium 2, we have

$$\frac{A^t_{f1}}{A^t_{s1}} = \delta_{p21}, \quad \frac{A^t_{f2}}{A^t_{s2}} = \delta_{p22}, \quad \text{and} \quad \frac{B^t_f}{B^t_s} = \delta_{s2}; \tag{A-8}$$

where

$$\delta_{pij} = \frac{\lambda^*_i + (\alpha^*_i)^2 M^*_i + 2\mu^*_i - \rho_{bi} V p^2_{ij}}{\rho_{fi} V^2_p - \alpha^*_i M^*_i} (i = 1,2; j = 1,2),$$

$$\delta_{si} = \frac{\mu^*_i - \rho_{bi} V^2_{si}}{\rho_{fi} V^2_{si}} (i = 1,2).$$

Here, $i = 1$ refers to the upper medium 1, and $i = 2$ refers to the lower medium 2; and $j = 1$ refers to the fast P-wave, and $j = 2$ refers to the slow P-wave. Consequently, V_{P11}, V_{P12}, V_{S1} and V_{P21}, V_{P22}, and V_{S2} are the frequency-dependent fast P-wave velocity, slow P-wave velocity, and S-wave velocity in the upper medium and lower medium, respectively.

If we substitute A-7 and A-8 into A-2, A-3, A-4, A-5, and A-6, we consequently have six unknown amplitudes of the displacement potentials A^r_{s1}, A^r_{s2}, B^r_s, A^t_{s1}, A^t_{s2}, and B^t_s, which correspond to the potential amplitudes of the reflected fast P-wave, reflected slow P-wave, reflected S-wave, transmitted fast P-wave, transmitted slow P-wave, and transmitted S-wave, respectively. Also, they are related to the six boundary conditions listed in equation 19–24.

Consequently, from the equations in A-1–A-8, we can relate the potential function to the displacement in media 1 and 2:

$$\begin{cases} u_{1x} = \frac{\partial(\varphi^i_s+\varphi^r_s)}{\partial x} - \frac{\partial\psi^r_s}{\partial z} = \frac{\partial(\varphi^i_s+\varphi^r_{s1}+\varphi^r_{s2})}{\partial x} - \frac{\partial\psi^r_s}{\partial z}, \\ u_{1z} = \frac{\partial(\varphi^i_s+\varphi^r_s)}{\partial z} + \frac{\partial\psi^r_s}{\partial x} = \frac{\partial(\varphi^i_s+\varphi^r_{s1}+\varphi^r_{s2})}{\partial z} + \frac{\partial\psi^r_s}{\partial x}, \\ W_{1x} = \frac{\partial(\varphi^i_f+\varphi^r_f)}{\partial x} - \frac{\partial\psi^r_f}{\partial z} = \frac{\partial(\delta_{p11}\varphi^i_s+\delta_{p11}\varphi^r_{s1}+\delta_{p12}\varphi^r_{s2})}{\partial x} - \delta_{s1}\frac{\partial\psi^r_s}{\partial z}, \\ W_{1z} = \frac{\partial(\varphi^i_f+\varphi^r_f)}{\partial z} + \frac{\partial\psi^r_f}{\partial x} = \frac{\partial(\delta_{p11}\varphi^i_s+\delta_{p11}\varphi^r_{s1}+\delta_{p12}\varphi^r_{s2})}{\partial z} + \delta_{s1}\frac{\partial\psi^r_s}{\partial x}, \end{cases} \tag{A-9}$$

$$\begin{cases} u_{2x} = \frac{\partial\varphi^t_s}{\partial x} - \frac{\partial\psi^t_s}{\partial z} = \frac{\partial(\phi^t_1+\phi^t_2)}{\partial x} - \frac{\partial\psi^t_s}{\partial z}, \\ u_{2z} = \frac{\partial\varphi^t_s}{\partial z} + \frac{\partial\psi^t_s}{\partial x} = \frac{\partial(\phi^t_1+\phi^t_2)}{\partial x} + \frac{\partial\psi^t_s}{\partial z}, \\ W_{2x} = \frac{\partial\varphi^t_f}{\partial x} - \frac{\partial\psi^t_f}{\partial z} = \frac{\partial(\delta_{p21}\phi^t_1+\delta_{p22}\phi^t_2)}{\partial x} - \delta_{s2}\frac{\partial\psi^t_s}{\partial z}, \\ W_{2z} = \frac{\partial\varphi^t_f}{\partial z} + \frac{\partial\psi^t_f}{\partial x} = \frac{\partial(\delta_{p21}\phi^t_1+\delta_{p22}\phi^t_2)}{\partial z} + \delta_{s2}\frac{\partial\psi^t_s}{\partial x}. \end{cases} \tag{A-10}$$

Following the boundary conditions listed in equations 19–24 and on the basis of the poroelastic stress-strain relationship, we have

$$u_{1x} = u_{2x}, \tag{A-11}$$

$$u_{1z} = u_{2z}, \tag{A-12}$$

$$(\lambda^*_1+\alpha^{*^2}_1 M^*_1)(u_{1x,x}+u_{1z,z})+2\mu_1 u_{1z,z}+\alpha_1 M^*_1(W_{1x,x}+W_{1z,z}) = (\lambda^*_2+\alpha^{*^2}_2 M^*_2)(u_{2x,x}+u_{2z,z})+2\mu^*_2 u_{2z,z}+\alpha^*_2 M^*_2(W_{2x,x}+W_{2z,z}), \tag{A-13}$$

$$\mu^*_1(u_{1x,z} + u_{1z,x}) = \mu^*_2(u_{2x,z} + u_{2z,x}), \tag{A-14}$$

$$W_{1z} = W_{2z}, \tag{A-15}$$

$$\alpha^*_1 M^*_1(u_{1x,x} + u_{1z,z}) + M^*_1(W_{1x,x} + W_{1z,z}) = \alpha^*_2 M^*_2(u_{2x,x} + u_{2z,z}) + M^*_2(W_{2x,x} + W_{2z,z}). \tag{A-16}$$

Note that the boundary conditions require that the phase factors must be equal at $z = 0$ for all x and t, and hence we have

$$k^i_{p1}\sin\theta^i x = k^r_{p1}\sin\theta^r_{p1} = k^r_{p2}\sin\theta^r_{p2} = k^r_s\sin\theta^r_s = k^t_{p1}\sin\theta^t_{p1} = k^t_{p2}\sin\theta^t_{p2} = k^t_s\sin\theta^t_s. \tag{A-17}$$

Equation A-17 is Snell's law for reflection and transmission in effective Biot media. Now, we substitute equations A-2–A-10 into the boundary condition A-11–A-16 and set $z = 0$ for all x and t. Then, we can obtain the Zoeppritz-style reflection and transmission coefficients of elastic waves from the boundary of effective Biot media, which are given in equations 25–28. Here, we define the reflection and transmission coefficients as the amplitude ratios for the matrix displacement.

REFERENCES

Adam, L., M. Batzle, and I. Brevik, 2006, Gassmann's fluid substitution and shear modulus variability in carbonates at laboratory seismic and ultrasonic frequencies: Geophysics, **71**, no. 6, F173–F183, doi: 10.1190/1.2358494.

Aki, K., and P. G. Richards, 1980, Quantitative seismology: Theory and methods: W. H. Freeman & Co..

Batzle, M. L., D. H. Han, and R. Hofmann, 2006, Fluid mobility and frequency-dependent seismic velocity — Direct measurements: Geophysics, **71**, no. 1, N1–N9, doi: 10.1190/1.2159053.

Berryman, J. G., and H. F. Wang, 1995, The elastic coefficients of double-porosity models for fluid transport in jointed rock: Journal of Geophysical Research, **100**, 24611–24627, doi: 10.1029/95JB02161.

Berryman, J. G., and H. F. Wang, 2000, Elastic wave propagation and attenuation in a double-porosity dual-permeability medium: International Journal of Rock Mechanics and Mining Sciences, **37**, 63–78, doi: 10.1016/S1365-1609(99)00092-1.

Biot, M. A., 1956a, Theory of propagation of elastic waves in fluid-saturated porous solid. I: Low-frequency range: Journal of the Acoustical Society of America, **28**, 168–178, doi: 10.1121/1.1908239.

Biot, M. A., 1956b, Theory of propagation of elastic waves in a fluid-saturated porous solid. II: Higher frequency range: Journal of the Acoustical Society of America, **28**, 179–191, doi: 10.1121/1.1908241.

Biot, M. A., 1962, Mechanics of deformation and acoustic propagation in porous media: Journal of Applied Physics, **33**, 1482–1498, doi: 10.1063/1.1728759.

Bourbié, T., 1983, Effects of attenuation on reflections: Ph.D. thesis, Stanford University.

Bourbié, T., O. Coussy, and B. Zinszner, 1987, Acoustics of porous media: Editions Technip.

Bourbié, T., and A. Nur, 1984, Effects of attenuation on reflections: Experimental test: Journal of Geophysical Research, **89**, 6197–6202, doi: 10.1029/JB089iB07p06197.

Bouzidi, Y., and D. R. Schmitt, 2012, Incidence-angle-dependent acoustic reflections from liquid-saturated porous solids: Geophysical Journal International, **191**, 1427–1440, doi: 10.1111/j.1365-246X.2012.05695.x.

Carcione, J. M., B. Gurevich, J. Santos, and S. Picotti, 2013, Angular and frequency-dependent wave velocity and attenuation in fractured porous media: Pure and Applied Geophysics, **170**, 1673–1683, doi: 10.1007/s00024-012-0636-8.

Carcione, J. M., and S. Picotti, 2006, P-wave seismic attenuation by slow wave diffusion: Effects of inhomogeneous rock properties: Geophysics, **71**, no. 3, O1–O8, doi: 10.1190/1.2194512.

Castagna, J. P., S. Sun, and R. W. Seigfried, 2003, Instantaneous spectral analysis: Detection of low-frequency shadows associated with hydrocarbons: The Leading Edge, **22**, 120–127, doi: 10.1190/1.1559038.

Castagna, J. R., H. W. Swan, and D. J. Foster, 1998, Framework for AVO gradient and intercept interpretation: Geophysics, **63**, 948–956, doi: 10.1190/1.1444406.

Downloaded 04/06/15 to 112.10.114.108. Redistribution subject to SEG license or copyright; see Terms of Use at http://library.seg.org/

Chakraborty, A., and D. Okaya, 1995, Frequency-time decomposition of seismic data using wavelet-based methods: Geophysics, **60**, 1906–1916, doi: 10.1190/1.1443922.
Chapman, M., S. V. Zatsepin, and S. Crampin, 2002, Derivation of a microstructural poroelastic model: Geophysical Journal International, **151**, 427–451, doi: 10.1046/j.1365-246X.2002.01769.x.
Chapman, M. E., E. Liu, and X. Li, 2006, The influence of fluid-sensitive dispersion and attenuation on AVO analysis: Geophysical Journal International, **167**, 89–105, doi: 10.1111/j.1365-246X.2006.02919.x.
Dai, Z., and Z. Kuang, 2006, Reflection and transmission of elastic waves from the interface of fluid-saturated porous solid and a double porosity solid: Transport in Porous Media, **65**, 237–264, doi: 10.1007/s11242-005-6084-5.
Denneman, A. I. M., G. G. Drijkoningen, D. M. J. Smeulders, and K. Wapenaar, 2002, Reflection and transmission of waves at a fluid/porous-medium interface: Geophysics, **67**, 282–291, doi: 10.1190/1.1451800.
Deresiewicz, H., and J. T. Rice, 1960, The effect of boundaries on wave propagation in liquid-filled porous solid. I: Reflection of plane waves at a true plane boundary (non-dissipative case): Bulletin of the Seismological Society of America, **50**, 599–607.
Dutta, N. C., and H. Odé, 1979a, Attenuation and dispersion of compressional waves in fluid-filled porous rocks with partial gas saturation (White model) Part I — Biot theory: Geophysics, **44**, 1777–1788, doi: 10.1190/1.1440938.
Dutta, N. C., and H. Odé, 1979b, Attenuation and dispersion of compressional waves in fluid filled porous rocks with partial gas saturation (White model) Part II — Results: Geophysics, **44**, 1789–1805, doi: 10.1190/1.1440939.
Dutta, N. C., and H. Odé, 1983, Seismic reflections from a gas-water contact: Geophysics, **48**, 148–162, doi: 10.1190/1.1441454.
Dvorkin, J., G. Mavko, and A. Nur, 1995, Squirt flow in fully saturated rocks: Geophysics, **60**, 97–107, doi: 10.1190/1.1443767.
Ebrom, D., 2004, The low frequency gas shadow on seismic sections: The Leading Edge, **23**, 772, doi: 10.1190/1.1786898.
Gassmann, F., 1951, Über die elastizität poröser medien: Vierteljahrsschrift der Naturforschenden Gesellschaft in Zürich, **96**, 1–23.
Geertsma, J., and D. C. Smit, 1961, Some aspects of elastic wave propagation in fluid-saturated porous solids: Geophysics, **26**, 169–181, doi: 10.1190/1.1438855.
Gelinsky, S., and S. A. Shapiro, 1997, Dynamic-equivalent medium approach for thinly layered saturated sediments: Geophysical Journal International, **128**, F1–F4, doi: 10.1111/j.1365-246X.1997.tb04086.x.
Goloshubin, G., C. Van Shuyver, V. Korneev, D. Silin, and V. Vingalov, 2006, Reservoir imaging using low frequencies of seismic reflections: The Leading Edge, **25**, 527–531, doi: 10.1190/1.2202652.
Goloshubin, G. M., T. M. Daley, and V. A. Korneev, 2001, Seismic low-frequency effects in gas reservoir monitoring VSP data: 71st Annual International Meeting, SEG, Expanded Abstracts, 1693–1696.
Gurevich, B., R. Ciz, and A. I. M. Denneman, 2004, Simple expressions for normal incidence reflection coefficients from an interface between fluid saturated porous materials: Geophysics, **69**, 1372–1377, doi: 10.1190/1.1836811.
Gurevich, B., and M. Schoenberg, 1999, Interface conditions for Biot's equations of poroelasticity: Journal of the Acoustical Society of America, **105**, 2585–2589, doi: 10.1121/1.426874.
Gurevich, B., V. B. Zyrianov, and S. L. Lopatnikov, 1997, Seismic attenuation in finely layered porous rocks: Effects of fluid flow and scattering: Geophysics, **62**, 319–324, doi: 10.1190/1.1444133.
Hofmann, H., 2006, Frequency-dependent elastic and anelastic properties of clastic rocks: Ph.D. thesis, Colorado School of Mines.
Johnson, D. L., J. Koplik, and R. Dashen, 1987, Theory of dynamic permeability and tortuosity in fluid-saturated porous media: Journal of Fluid Mechanics, **176**, 379–402, doi: 10.1017/S0022112087000727.
Korneev, V. A., G. M. Goloshubin, T. M. Daley, and D. B. Silin, 2004, Seismic low-frequency effects in monitoring fluid-saturated reservoirs: Geophysics, **69**, 522–532, doi: 10.1190/1.1707072.
Lines, L., K. Innanen, F. Vasheghani, J. Wong, C. Sondergeld, S. Treitel, and T. Ulrych, 2012, Experimental confirmation of "Reflections on Q": 82nd Annual International Meeting, SEG, Expanded Abstracts, 10.1190/segam2012-0187.1.
Lines, L., F. Vasheghani, and S. Treitel, 2008, Reflections on Q: CSEG Recorder, **33**, 36–38.
Liu, L., S. Cao, and L. Wang, 2011, Poroelastic analysis of frequency-dependent amplitude-versus-offset variations: Geophysics, **76**, no. 3, C31–C40, doi: 10.1190/1.3552702.
Masson, Y. J., and S. R. Pride, 2007, Poroelastic finite-difference modeling of seismic attenuation and dispersion due to mesoscopic-scale heterogeneity: Journal of Geophysical Research, **112**, B10305, doi: 10.1029/2006JB004592.
Mavko, G., and D. Jizba, 1991, Estimating grain-scale fluid effects on velocity dispersion in rocks: Geophysics, **56**, 1940–1949, doi: 10.1190/1.1443005.
Mavko, G., T. Mukerji, and J. Dvorkin, 2009, The rock physics handbook, 2nd ed.: Cambridge University Press.
Mavko, G., and A. Nur, 1975, Melt squirt in the asthenosphere: Journal of Geophysical Research, **80**, 1444–1448, doi: 10.1029/JB080i011p01444.
Morozov, I., 2011, Anelastic acoustic impedance and the correspondence principle: Geophysical Prospecting, **59**, 24–34, doi: 10.1111/j.1365-2478.2010.00890.x.
Müller, T. M., and B. Gurevich, 2004, One-dimensional random patchy saturation model for velocity and attenuation in porous rocks: Geophysics, **69**, 1166–1172, doi: 10.1190/1.1801934.
Müller, T. M., and B. Gurevich, 2005, Wave induced fluid flow in random porous media: Attenuation and dispersion of elastic waves: Journal of the Acoustical Society of America, **117**, 2732–2741, doi: 10.1121/1.1894792.
Müller, T. M., B. Gurevich, and M. Lebedev, 2010, Seismic wave attenuation and dispersion resulting from wave-induced flow in porous rocks: A review: Geophysics, **75**, no. 5, A147–A164, doi: 10.1190/1.3463417.
Müller, T. M., G. Lambert, and B. Gurevich, 2007, Dynamic permeability of porous rocks and its seismic signatures: Geophysics, **72**, no. 5, E149–E158, doi: 10.1190/1.2749571.
O'Connell, R. J., and B. Budiansky, 1974, Seismic velocities in dry and saturated cracked solids: Journal of Geophysical Research, **79**, 5412–5426, doi: 10.1029/JB079i035p05412.
Odebeatu, E., J. Zhang, M. Chapman, E. Liu, and Y. Li, 2006, Application of spectral decomposition to detection of dispersion anomalies associated with gas saturation: The Leading Edge, **25**, 206–210, doi: 10.1190/1.2172314.
Partyka, G., J. Gridley, and J. Lopez, 1999, Interpretational applications of spectral decomposition in reservoir characterization: The Leading Edge, **18**, 353–360, doi: 10.1190/1.1438295.
Pride, S. R., and J. G. Berryman, 2003a, Linear dynamics of double-porosity and dual-permeability materials. I: Governing equations and acoustic attenuation: Physical Review E, **68**, 036603, doi: 10.1103/PhysRevE.68.036603.
Pride, S. R., and J. G. Berryman, 2003b, Linear dynamics of double-porosity and dual permeability materials. II: Fluid transport equations: Physical Review E, **68**, 036604, doi: 10.1103/PhysRevE.68.036604.
Pride, S. R., J. G. Berryman, and J. M. Harris, 2004, Seismic attenuation due to wave induced flow: Journal of Geophysical Research, **109**, B01201, doi: 10.1029/2003JB002639.
Pride, S. R., E. Tromeur, and J. G. Berryman, 2002, Biot slow-wave effects in stratified rock: Geophysics, **67**, 271–281, doi: 10.1190/1.1451799.
Quintal, B., S. M. Schmalholz, and Y. Y. Podladchikov, 2009, Low-frequency reflections from a thin layer with high attenuation caused by interlayer flow: Geophysics, **74**, no. 1, N15–N23, doi: 10.1190/1.3026620.
Quintal, B., H. Steeb, M. Frehner, S. M. Schmalholz, and E. H. Saenger, 2012, Pore fluid effects on S-wave attenuation caused by wave-induced fluid flow: Geophysics, **77**, no. 3, L13–L23, doi: 10.1190/GEO2011-0233.1.
Ren, H., G. Goloshubin, and F. J. Hilterman, 2009, Poroelastic analysis of amplitude-versus-frequency variations: Geophysics, **74**, no. 6, N41–N48, doi: 10.1190/1.3207863.
Rubino, J. G., C. L. Ravazzoli, and J. E. Santos, 2006, Reflection and transmission of waves in composite porous media: A quantification of energy conversions involving slow waves: Journal of the Acoustical Society of America, **120**, 2425–2436, doi: 10.1121/1.2354464.
Rubino, J. G., C. L. Ravazzoli, and J. E. Santos, 2009, Equivalent viscoelastic solids for heterogeneous fluid-saturated porous rocks: Geophysics, **74**, no. 1, N1–N13, doi: 10.1190/1.3008544.
Rutherford, S. R., and R. H. Williams, 1989, Amplitude-versus-offset variations in gas sands: Geophysics, **54**, 680–688, doi: 10.1190/1.1442696.
Shapiro, S. A., and T. M. Müller, 1999, Seismic signatures of permeability in heterogeneous porous media: Geophysics, **64**, 99–103, doi: 10.1190/1.1444536.
Stoll, R. D., 1977, Acoustic waves in ocean sediments: Geophysics, **42**, 715–725, doi: 10.1190/1.1440741.
Taner, M. T., F. Koehler, and R. E. Sheriff, 1979, Complex seismic trace analysis: Geophysics, **44**, 1041–1063, doi: 10.1190/1.1440994.
Tang, X., 2011, A unified theory for elastic wave propagation through porous media containing cracks: An extension of Biot's poroelastic wave theory: Science China — Earth Sciences, **54**, 1441–1452, doi: 10.1007/s11430-011-4245-7.
Tang, X. M., and C. H. Cheng, 2004, Quantitative borehole acoustic methods: Elsevier Science Publishing Co.
Vernik, L., 1994, Hydrocarbon-generation-induced microcracking of source rocks: Geophysics, **59**, 555–563, doi: 10.1190/1.1443616.
Walton, K., 1987, The effective elastic moduli of a random pack of spheres: Journal of the Mechanics and Physics of Solids, **35**, 213–226, doi: 10.1016/0022-5096(87)90036-6.
Wenzlau, F., J. B. Altmann, and T. M. Müller, 2010, Anisotropic dispersion and attenuation due to wave-induced fluid flow: Quasi-static finite element

modeling in poroelastic solids: Journal of Geophysical Research, **115**, B07204, doi: 10.1029/2009JB006644.
White, J. E., 1965, Reflections from lossy media: Journal of the Acoustical Society of America, **38**, 604–607, doi: 10.1121/1.1909756.
White, J. E., 1975, Computed seismic speeds and attenuation in rocks with partial gas saturation: Geophysics, **40**, 224–232, doi: 10.1190/1.1440520.
Yao, Q., 2013, Velocity dispersion and attenuation in reservoir rocks: Ph.D. thesis, University of Houston.
Yao, Q., D. Han, F. Yan, and L. Zhao, 2013, Fluid substitution with dynamic fluid modulus: Facing the challenges in heterogeneous rocks: 83rd Annual International Meeting, SEG, Expanded Abstracts, 2851–2855.

Downloaded 04/06/15 to 112.10.114.108. Redistribution subject to SEG license or copyright; see Terms of Use at http://library.seg.org/